

# The Effects of pH and Chelating Agent on Synthesis and Characterization of Ni Mo/ $\gamma$ - Alumina Nanocatalyst for Heavy Oil Hydrodesulfurization

*Sheibani, Soheila; Zare, Karim\*<sup>+</sup>*

*Department of Chemistry, Science and Research Branch, Islamic Azad University, Tehran, I.R. IRAN*

*Mousavi Safavi, Seyed Mahmood*

*Department of Chemistry and Chemical Engineering, Buin Zahra Branch, Islamic Azad University, Buin Zahra, I.R. IRAN*

**ABSTRACT:** *In this research, various organic additives (as a chelating agent) were used to prepare NiMo/  $\gamma$ -Al<sub>2</sub>O<sub>3</sub> bimetallic catalysts. Then effects of additives and pH variation were studied on textural properties, morphology and size of nanocatalyst particles, interaction, and loading of active metals on a support. Additionally, this research evaluated the activity of catalysts and compared them with commercial and catalysts in the absence of additives. The metal oxide nanoparticles were prepared and impregnated on  $\gamma$ -Al<sub>2</sub>O<sub>3</sub> in-situ by using the wetness impregnation method, under conditions 60°C and calcination temperature 520°C. The supported nanocatalyst was calcined to remove the volatile materials and gases. The catalysts were characterized by TPR, BET, BJH, AAS, FT-IR, SEM, and XRD. The prepared nanocatalyst displayed the enhanced catalytic activity for the heavy oil hydrodesulfurization (HDS) containing 21 g/L sulfur. At the acidic pH, the activity of the catalyst was promoted by using EDTA compound as a chelating agent. The sulfur content of the feed was decreased up to 2 g/L at 380°C, 60 bar, and LHSV 1.5h<sup>-1</sup> showing an efficient catalyst with the conversion of 90.47%.*

**KEYWORDS:** *Molybdenum oxide; Nickel oxide; Nanostructures; Hydrodesulfurization; Chelating agent; Heavy oil.*

## INTRODUCTION

Nowadays, to prevent air pollution, it is necessary to reduce sulfur in the liquid motor fuels [1, 2]. The elimination of sulfur content in the fuel products is carried out by using the conventional hydrodesulfurization (HDS) process as a main industrial process. For HDS process, numerous active catalysts have been produced through several techniques, such as in situ activation in the presence

of a hydrocarbon solvent [1] and modification of support [2-7]. *Shahidian et al.* [5, 7] prepared a specific type of mesopore extrudates gamma alumina. They conducted modification with acidic or alkaline treatment. to improve the catalytic properties, various additives such as phosphorus, fluorine and lanthanum have been added to the  $\gamma$ -Al<sub>2</sub>O<sub>3</sub> support [2]. Additionally, using new supports

---

\* To whom correspondence should be addressed.

+ E-mail: k-zare@sbu.ac.ir

1021-9986/2021/1/21-34

14/\$/6.04

with specific physiochemical properties, such as nano porous carbon increased the activity of the catalyst. One of the strategies is to develop novel carrier, resulting in more efficient hydrotreating catalysts. This can contribute in obtaining enhanced properties of supported sulfide CoMo or NiMo active phases [3]. Such hydrodesulfurization of dibenzothiophene and gas oil have been carried out on ASA-supported TMS (transition metal sulphides) under industrial conditions approach [4]. Another strategy is the application of unsupported catalysts for the HDS of oil feed, such as unsupported  $\text{MoO}_3$  nanostructure [8], unsupported Ni-Zn-Mo catalyst [9], and unsupported materials with higher activity and/or selectivity. They perform better than the traditional supported Ni/Co-Mo/W/ $\gamma$ - $\text{Al}_2\text{O}_3$  catalysts [10-11], and Mo nanoparticles using  $\gamma$ -radiation [12]. Since prepared catalysts are not always able to perform deep HDS of oil feed, the challenge is to design new catalysts, which could be more effective for deep S-removal. Also, they could be sustainable and recyclable [13, 14]. In recent years, there has been a considerable interest in the synthesis and characterization of heterogeneous nanoparticles. These nanoparticles often show novel properties, which are different from the bulk materials. The improvement of the characteristics of the HDS catalysts and nanoparticle impregnation as an active site on support was done by adding a chelating agent to the impregnation solution [15-19]. As an example, *Suarez-Toriello et al.* [19] prepared NiW/ $\gamma$ - $\text{Al}_2\text{O}_3$  catalysts by using citric acid as a chelating agent. They studied the effect of nickel-citric acid solution pH on metal-support interactions. They obtained suitable condition for the formation of the sulfide phase to achieve high catalytic activity in the HDS of 4,6-dimethyl dibenzothiophene (4,6-DMDBT). Another more efficient method is to prepare ultra-small NiMo bimetallic nano clusters on  $\gamma$ - $\text{Al}_2\text{O}_3$  to achieve high activity catalyst [20]. NiMo/ $\gamma$ - $\text{Al}_2\text{O}_3$  catalyst is applied to the other processes as well. Recently, to use biofuels instead of fossil fuels in the presence of high oxygenated compound, many studies have been conducted on the removal of these components. *Hoceva et al.* [21] applied Ni-Mo/ $\text{Al}_2\text{O}_3$  catalyst to study the kinetics of hydrodeoxygenation (HDO) of the model organic compound. They investigated on oxygenated functional groups in hexane as a model compound. Additionally, *Hoceva et al.* [22] continued their studies on the removal of oxygenated materials in linear  $\text{C}_6$  ketones

and secondary alcohols. *Grilc et al.* [23] reported HDO of levolenic acid by using Ni-Mo/ $\text{Al}_2\text{O}_3$  catalyst, investigated reaction kinetics and determined the effects of different parameters on the reaction rate. Moreover, some researchers have evaluated the replacement of fixed bed reactors, commonly used for HDS process, with slurry reactors. For example, *Khadem-Hamedani et al.* [24] reported a mathematic model via slurry bubble column reactor for HDS process over NiMoS/ $\text{Al}_2\text{O}_3$  catalyst and compared performance of single- and two-class models in the HDS of DBT.

The main aim of this study was to synthesize a catalyst with a better performance. Therefore, enhancing the activity of the HDS catalyst was investigated. Based on the properties of nanoparticles,  $\text{MoO}_3$  and NiO nanostructure were synthesized, by using organic additives as chelating agent and supported on  $\gamma$ - $\text{Al}_2\text{O}_3$ . This catalyst is suitable for heavy feed. Furthermore, the effects of impregnation conditions such as media pH and type of organic additives on textural properties, size of nanocatalyst particles, interaction and loading of active metals on support and catalyst performance were precisely investigated.

## EXPERIMENTAL SECTION

### Materials

To prepare NiMo/ $\gamma$ - $\text{Al}_2\text{O}_3$  catalysts, the first precursor was a  $\gamma$ - $\text{Al}_2\text{O}_3$  (surface area  $250 \text{ m}^2/\text{g}$ , pore volume  $0.78 \text{ cm}^3/\text{g}$ , pore diameter  $12.6 \text{ nm}$ ). It was purchased from Azarshahr Nephelinsinite mine ores as internal source and typically used as a support. The other precursors were ammonium hepta molybdate, AHM,  $(\text{NH}_4)_6\text{Mo}_7\text{O}_{24}\cdot 4\text{H}_2\text{O}$ , nickel nitrate  $(\text{Ni}(\text{NO}_3)_2\cdot 6\text{H}_2\text{O})$ , citric acid ( $\text{C}_6\text{H}_8\text{O}_7$ ), Ethylene Diamine Tetra Acetic acid (EDTA), Poly Ethylene Glycol (PEG) and urea  $(\text{NH}_4)_2\text{CO}$ . They were laboratory grade (with purities of 98% to 100%) from Merck, Germany.

### Characterization techniques

Metal contents were determined by using Atomic Absorption Spectrometry (AAS) (GBC Avanta Absorption) according to ASTM D 4698. 0.1 gr of samples were dissolved in the 100 mL of  $\text{H}_2\text{SO}_4$  solution. Then the absorbance was determined. The phase structure of the samples was investigated by using X-ray Diffraction (X'pertpro from analytical company diffractometer). It was equipped with a Cu  $K\alpha$  radiation source ( $\lambda = 1.540596 \text{ \AA}$ )

and  $2\theta$  was in the range of ( $5^\circ - 80^\circ$ ). The step size was  $0.026^\circ$ , time/step was 10s, and conditions were at 40 mA and 40kV. Additionally, the pore structure of the samples was measured by using  $N_2$ -adsorption/desorption porosimetry (Belsorp mini II, BEL JAPAN) according to ASTM: ISO 15901-2-2006 and ISO 15901-3-2007). Prior to any measurements, all samples were degassed (under vacuum at the temperature of  $250^\circ\text{C}$ ) for 3h. The  $N_2$ -adsorption/desorption isotherms were used to calculate the Brunauer–Emmett–Teller (BET) specific surface area. Pore volume and pore diameter distribution were computed by using the Barrett–Joyner–Halenda (BJH) technique.

Temperature-Programmed Reduction (TPR) profiles were obtained on a Micromeritic–2900 apparatus interfaced with a computer. 0.1 g of a sample was housed in a quartz tubular reactor. The TPR profiles were obtained by passing a 10%  $H_2/Ar$  flow (22 mL/min) through the sample in the temperature range of ( $30^\circ\text{C} - 1000^\circ\text{C}$ ). In that case, the temperature was increased with a rate of  $10^\circ\text{C min}^{-1}$  and the hydrogen consumption was measured with a Thermal Conductivity Detector (TCD). In addition, FT-IR spectra were obtained in the wavenumber range of ( $400-4000$ )  $\text{cm}^{-1}$  with a resolution of  $1 \text{ cm}^{-1}$  (Unicam Matson 1000). 10 mg of the catalyst sample was added to 200 mg of KBr and rubbed in a mortar. As a result, one pellet was made. Then the pellet was placed in the instrument to get the infrared spectra [25]. The total sulfur in every sample was determined by Rigaku devices (U.S.A.) with semi-conductor Silicon PIN diode detector according to ASTM D: 4294. Surface morphology and particle size of the catalysts were determined by using field emission scanning electron microscopy (FE-SEM) by MIRA 3 TESCAN.

#### **Catalyst preparation**

All the nanocatalysts were prepared by wetness method. Two impregnation solutions were prepared by using 0.5 g of AHM and 0.4 gr of nickel nitrate in 10 mL of distilled water, and specific amount of chelate agent in 10 mL of distilled water. The pH of the solution was adjusted on 4. The molar ratio of a chelating agent to Mo was 1.2 for all the additives [26]. After contacting  $\gamma\text{-Al}_2\text{O}_3$  support with the impregnating solution for 6h, the excess water was evaporated at the temperature of  $60^\circ\text{C}$ . Then catalysts were dried in an oven at the temperature of  $120^\circ\text{C}$

for 2h. It was calcined in a 2-step procedure by using a furnace. Firstly, the temperature programming rate was at the rate of  $2^\circ\text{C min}^{-1}$ . The temperature was maintained at  $300^\circ\text{C}$  for 2h. Then it was increased up to  $520^\circ\text{C}$  and isothermal calcination was conducted for 5h. The Table 1 shows typical catalyst composition.

#### **Catalyst bench scale reactor test**

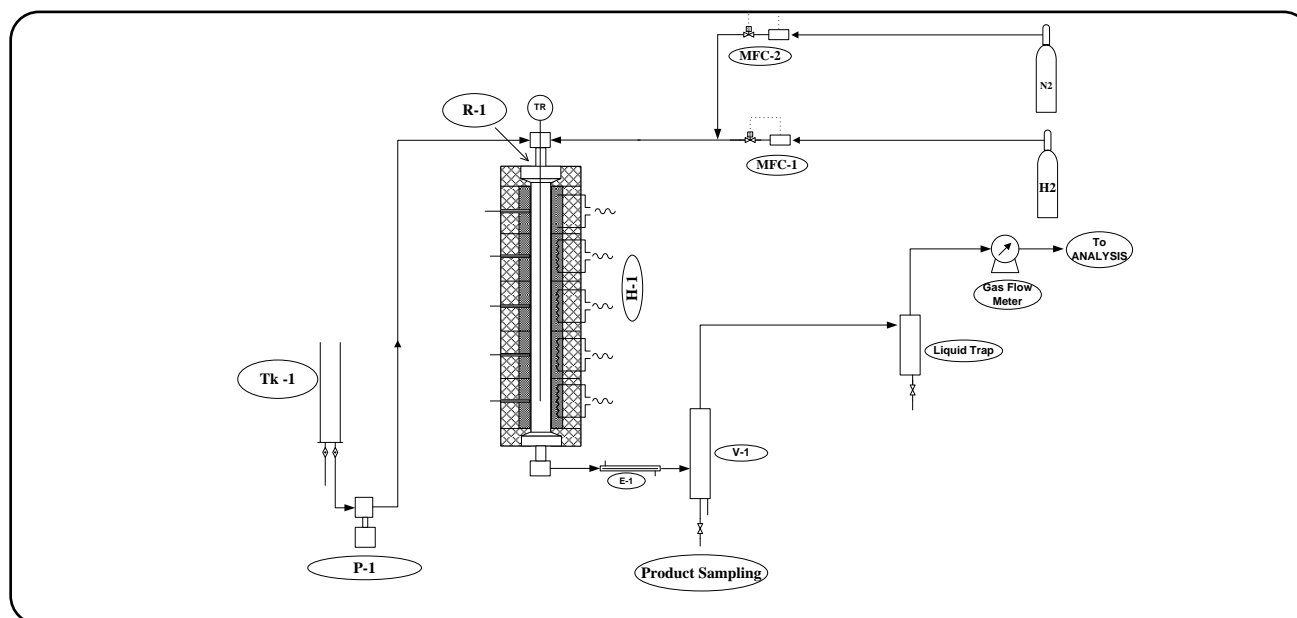
The HDS reaction of a 50/50 diluted heavy oil and gas oil feed with 21 g/L sulfur was performed in a low-pressure laboratory scale. Under these circumstances, set-up was equipped with a stainless-steel fixed bed catalytic reactor (20 mm i.d. and 230 mm length). For the HDS of heavy oil, the reaction conditions were  $T=400^\circ\text{C}$ ,  $P=60$  barg,  $LHSV=1.5\text{h}^{-1}$ ,  $H_2/H.C. = 1000\text{Nm}^3/\text{m}^3$ , and 5g of the catalyst. The sulfide form of the  $\text{NiMo}/\gamma\text{-Al}_2\text{O}_3$  catalyst was regarded as the active form; therefore, the catalyst was undergone sulfiding before evaluating the HDS activity of the catalyst by using 2wt% of dimethyl disulfide (DMDS) dissolved in gas oil. The flow rate of hydrogen and the liquid were 13.5 L/h and 13.5 mL/h, respectively. Before acquiring the conversion data, the catalyst was stabilized for at least 12 h [20]. Fig. 1 and Table 2 show the schematic of the reactor test and composition of the typical feed, respectively.

## **RESULTS AND DISCUSSION**

Since a catalyst with the further activity was required for the HDS reaction of a heavy oil feed, the  $\text{NiMo}/\gamma\text{-Al}_2\text{O}_3$  catalyst was prepared. Then the effects of organic additives and the pH of the media were investigated on the characterization of the catalyst. The performance test was conducted in a low pressure laboratory scale – up. Afterwards, the activity was compared with commercial and no additive catalysts. For synthesis, the  $\text{MoO}_3$  nanoparticle was used from AHM, which is usually used as a source in the preparation of molybdenum compounds [8]. Also, nitrate nickel was used as a precursor in NiO compound preparation. The chelating agent role in the enhancing of HDS activity is to form highly active sites through  $\text{MoO}_3$  nucleus formation, to grow them, and to move them to nanoparticles. Since the heavy oil feedstock contains heavy materials with large molecules, a support with high pore diameter should be used to allow big molecules to diffuse in the catalyst active sites. If the pore diameter is enlarged, the surface area will decrease and

**Table 1: Composition of the hydrodesulfurization catalyst that is measured with XRF typically**

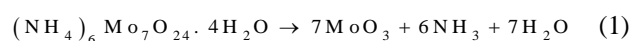
| Component | SiO <sub>2</sub> | Al <sub>2</sub> O <sub>3</sub> | Fe <sub>2</sub> O <sub>3</sub> | CaO  | MoO <sub>3</sub> | NiO  | TiO <sub>2</sub> | MnO   | MgO  | OK <sub>2</sub> | ONa <sub>2</sub> | P <sub>2</sub> O <sub>5</sub> | S     | Loss Of Ignition |
|-----------|------------------|--------------------------------|--------------------------------|------|------------------|------|------------------|-------|------|-----------------|------------------|-------------------------------|-------|------------------|
| Wt%       | 0.62             | 69.58                          | 2.01                           | 0.26 | 10.65            | 4.02 | 0.087            | 0.006 | 0.09 | 0.02            | 0.07             | 0.015                         | 0.342 | 12.04            |

**Fig 1: Schematic of the reactor test.****Table 2: Composition of the typical feed.**

| Specification            | Result |
|--------------------------|--------|
| Density (15.6 C)         | 0.998  |
| S (wt. %)                | 4.03   |
| N <sub>2</sub> (wt. ppm) | 3610   |
| CCR (wt. ppm)            | 15.5   |
| Ni (wt. ppm)             | 40.6   |
| V (wt. ppm)              | 126    |

catalyst activity will decrease. As a result, by using chelate agent to produce nanoparticles with good dispersion feature, one can improve catalytic activity. Also, the chelating agents consume NiMoO<sub>4</sub> that is not a good promoter for NiMoS-type structures and redistributes of Ni<sup>2+</sup> cations on the surface [27]. The researches have shown that the addition of the chelate agents do not increase the dispersion of Mo and the number of CUS (coordinately unsaturated sites) [17]. It can be concluded that the higher activities of nano clusters on  $\gamma$ -Al<sub>2</sub>O<sub>3</sub>

may be because of the high dispersion or smaller particle size in comparison with the non-nano catalyst. The smaller size of the crystals leads to a greater number of CUS or anion sites. These anion vacancies or CUS sites result in HDS catalytic activities; therefore, the nanoparticles on the  $\gamma$ -Al<sub>2</sub>O<sub>3</sub> supported catalysts have higher activities. Alternatively, the following reaction of the AHM molecules in solution completes without organic additives. And with heating lead to reaction. The molecules are bounded to form a long molecular chain. However, when organic additives are used as chelating agents in a reaction, distances between particles will be created. Organic additives will direct MoO<sub>3</sub> nucleus formation and growth (Eq. (1)).



HDS catalysts are based on molybdenum sulfide, along with a small amount of promoters. There are two types of active sites for MoS<sub>2</sub>. The hydrogenation carried out on rim sites and HDS on rim and edge sites [44]. The crystalline structure of catalyst contains bridges of sulfur with Mo

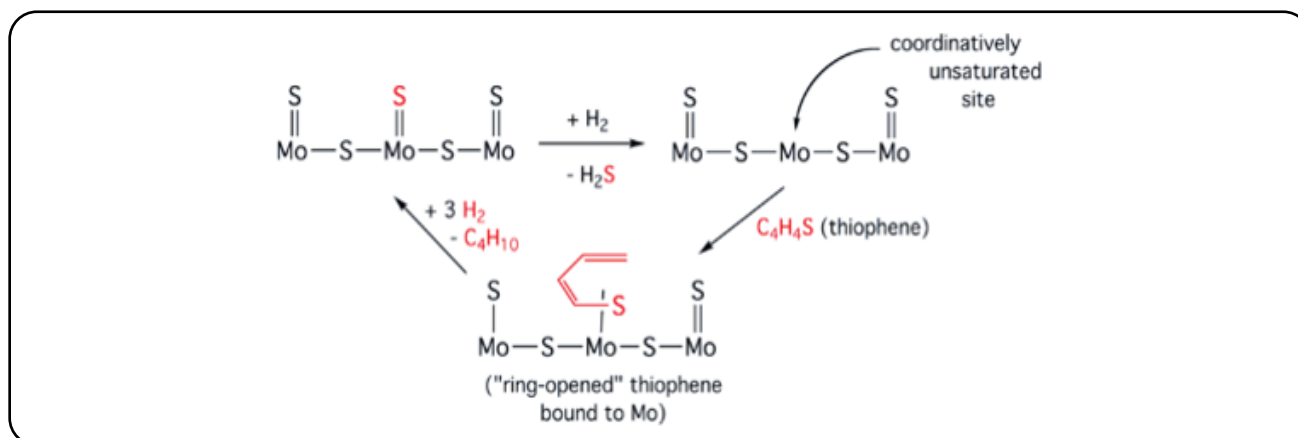
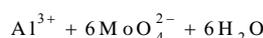
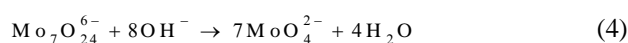
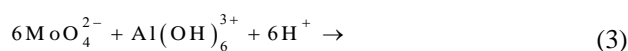
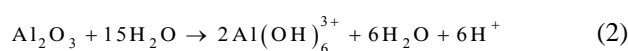


Fig. 2: Schematic of the hydrodesulfurization reaction mechanism of a hydrocarbon with a catalyst typically

in the center and unsaturated active sites. In the same way, in the bonding of sulfur compounds with active sites, C=S bond is broken, hydrogenolysis is occurred, and C=C bond is hydrogenated. Therefore, the reaction of H<sub>2</sub> with sulfur of catalyst and elimination of H<sub>2</sub>S activate the reaction sites again. H<sub>2</sub> has responsibility of hydrogenation, hydrogenolysis, and generation of anionic active site. Fig. 2 shows mechanism of the reaction [28].

In the HDS catalysts, precursor concentration determines the type of molecular structure of Mo. As an example, if the concentration of molybdenum is less than 3 wt% in the solution, four- coordinate monomeric structure of Mo is obtained (MoO<sub>4</sub><sup>2-</sup>) [29-31] after the calcination process. When the concentration of Mo in solution is more than 7 wt%, the polymer structure with six- coordinate of Mo tends to be formed (MoO<sub>3</sub>). On the other hand, the molecular structures depend on the pH of Mo solution. With this intention, in low concentration and pH >4 four (MoO<sub>4</sub><sup>2-</sup>), six-coordinate monomeric species [MoO<sub>2</sub>(OH)<sub>2</sub>(H<sub>2</sub>O)<sub>2</sub>] are produced [32]. At the high concentration of Mo, octa and hepta structures are produced [32-33]. In the presence of free ions of Al<sup>3+</sup>, a special structure is represented by the [Al(OH)<sub>6</sub>Mo<sub>6</sub>O<sub>18</sub>]<sup>3-</sup> or [AlMo<sub>6</sub>] formula. According to the following reactions (Eqs. (2) and (3)), Al ions are produced by dissolving Al<sub>2</sub>O<sub>3</sub>. Finally, the mentioned ion is formed through the reaction Al ions with MoO<sub>4</sub><sup>2-</sup> [34]. The stoichiometry calculation shows that when the concentration of Mo is more than 6.3 wt%, AlMo<sub>6</sub> is produced when Mo less than 6.3 wt%, hepta molybdat species are dominant in the catalysts [34]. Also, according to the reactions 4 and 5, the polymer structure can be converted to monomer structure on the surface of the catalyst.



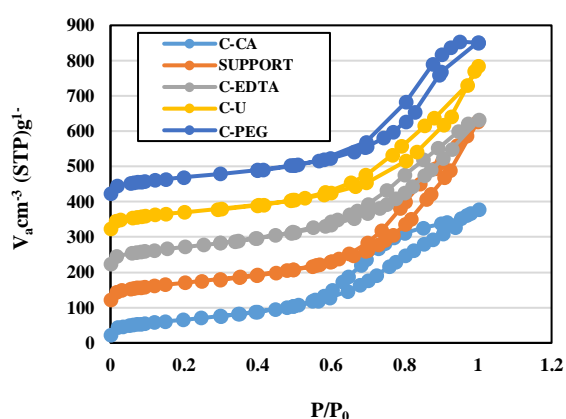
#### The effect of organic additives as chelating agent

Previous researches evaluated the effect of various organic additives on MoO<sub>3</sub> nanoparticle formation and growth [2]. In this research, four organic additives, including PEG, EDTA, citric acid, and urea were selected based on size, ligand dents, and acidity. They were followed by the examination and investigation of their effects on MoO<sub>3</sub> and NiO nanoparticles and loading of active metal on support and specification of catalyst. Therefore, it was impregnated on support from impregnation of solution as well as the chemical and textural properties of the catalyst were investigated. All the additives were examined in similar reaction conditions.

The pH of the reaction medium was less than 7, the synthesis temperature was kept at 60°C, and calcination temperature was kept at 520°C. The results of these experiments are briefly presented in Fig. 3 and Table 3. Catalyst with citric acid, EDTA, urea, and polyethylene

**Table 3: Physicochemical properties of prepared catalysts. The results show increasing of surface area in the C-EDTA.**

| catalyst | BET                                            |                                                |                            | BJH-ads                                        |                  |                                                | BJH-des                                        |                  |                                                | Chemical properties |       |
|----------|------------------------------------------------|------------------------------------------------|----------------------------|------------------------------------------------|------------------|------------------------------------------------|------------------------------------------------|------------------|------------------------------------------------|---------------------|-------|
|          | Surface Area (m <sup>2</sup> g <sup>-1</sup> ) | Pore Volume (cm <sup>3</sup> g <sup>-1</sup> ) | Average Pore Diameter (nm) | Pore Volume (cm <sup>3</sup> g <sup>-1</sup> ) | Pore Radius (nm) | Surface Area (m <sup>2</sup> g <sup>-1</sup> ) | Pore Volume (cm <sup>3</sup> g <sup>-1</sup> ) | Pore Radius (nm) | Surface Area (m <sup>2</sup> g <sup>-1</sup> ) | MoO <sub>3</sub> %  | NiO % |
| C-U      | 218                                            | 0.6318                                         | 10.62                      | 0.63                                           | 4.62             | 259.43                                         | 0.63                                           | 4.62             | 259.43                                         | 10.5                | 2.6   |
| C-CA     | 238                                            | 0.57                                           | 9.5                        | 0.5756                                         | 3.1              | 281.53                                         | 0.6                                            | 2.73             | 346.58                                         | 22.76               | 3.34  |
| C-PEG    | 247                                            | 0.68                                           | 11.07                      | 0.6825                                         | 4.62             | 267.4                                          | 0.71                                           | 3.54             | 305.39                                         | 24.2                | 3.5   |
| C-EDTA   | 250                                            | 0.64                                           | 9.9                        | 0.6443                                         | 2.12             | 280.2                                          | 0.66                                           | 3.1              | 290.37                                         | 36                  | 4.22  |
| SUPPORT  | 253                                            | 0.78                                           | 12.46                      | 0.788                                          | 4.62             | 283                                            | 0.81                                           | 4.04             | 317.7                                          | -                   | -     |

**Fig. 3: N<sub>2</sub>-adsorption/desorption isotherms of synthesized catalysts in presence of different various chelate agent in same condition**

glycol are denoted C-CA, C-EDTA, C-U, and C-PEG, respectively. The results show increase in the surface area of C-EDTA.

The results in the Table 3 show reducing pore volume ( $v_p$ ) of catalyst comparing with support, so active metals are located in the pores. Comparing  $v_p$  – ads and  $v_p$  – des displays being pores cylindrically. All of the catalysts show N<sub>2</sub>- adsorption/desorption isotherms with hysteresis loop as IV type isotherm in terms of IUPAC classification. Shape of hysteresis loop shows protected cylindrical pores, so we can conclude uniform dispersion of active metals in the pores. Also, comparing  $r_p$  – ads and  $r_p$  – des reveals, reducing percent of pore size from urea to EDTA is less. Therefore, we can conclude particle size of metal active have been enlarged. The results show that the performance of EDTA is better than other additives in the nucleus formation of impregnation solution and interaction of active metal with support. So, the properties of the catalyst have been improved. According to the effect of the chelating agent on the formation of highly active sites

and morphology of MoO<sub>3</sub> particle, the increase in surface area may not match with the average pore diameter. Trend of increasing of surface area in terms of additive as follows: C-U ≤ C-CA < C-PEG < C-EDTA. Obviously, increasing surface area reduces the average pore diameter, so it has been reduced in the C-EDTA catalyst. This means that EDTA is a useful amino carboxylic acid because it plays the role of a six-dent ligand and its chelating function can separate metal ions. Afterwards, metal ions can bind with EDTA and remain in the solution. The main functional groups in EDTA are two nitrogen atoms and four oxygen atoms. Therefore, further ions were removed from the complex and impregnated on the support. The active sites were increased. Citric acid, which has four oxygen atoms, can bond with metal. However, in urea, only two nitrogen atoms (functional groups) can extract Mo ions from the AHM complex structure.

The SEM images of nanocatalysts are shown in the Fig. 4. These results confirm mentioned analysis. It can be seen that the morphology of all catalysts leads to spherical nanoparticles and particle size of catalysts is less than 100 nm when chelate agent is used in the preparation of catalysts. Comparison of SEM images of catalysts shows that the active metals are oligomerated in the absence chelate agent (Fig. 4a) or weak chelate agent (Fig. 4b). These results are consistent with the performance test and surface area results.

#### **The effect of impregnation solution pH**

The pH of impregnation solution is an important parameter in catalyst synthesis. The influence of pH on catalyst characteristics depends on the nature of the additive when it is used in the catalyst solution, [8]. In the other words, the presence of H<sup>+</sup> or OH<sup>-</sup> groups

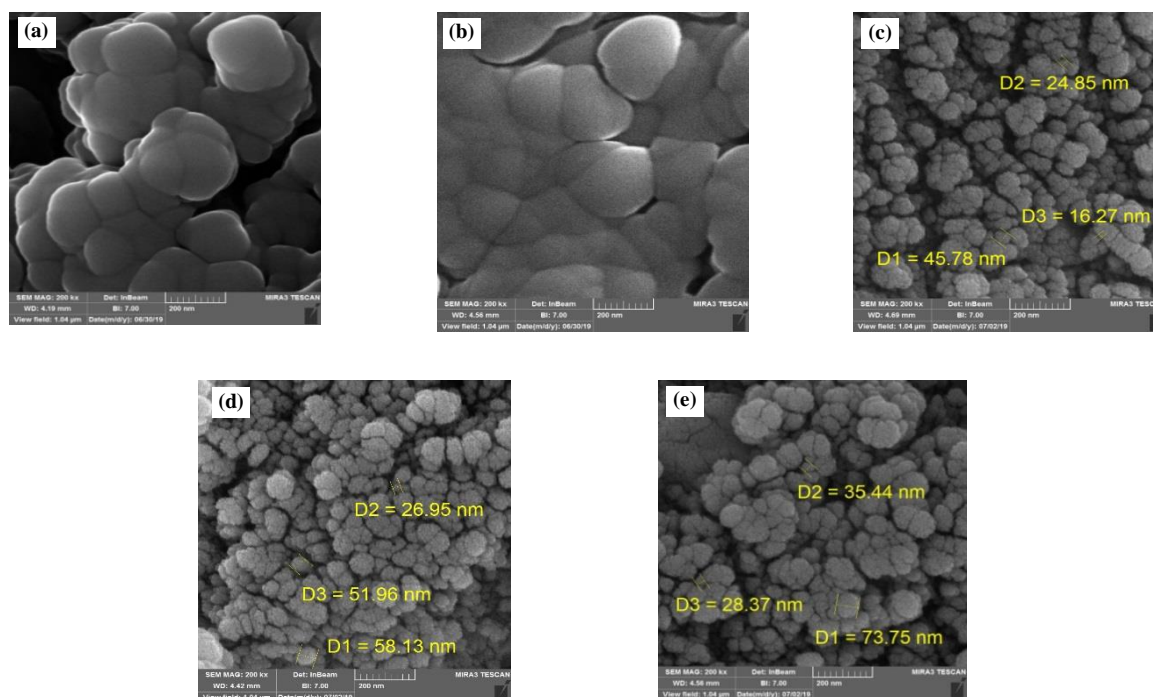


**Fig. 4:** SEM images of the nano catalysts prepared in presence/absence chelate agent, (a) is C-0, (b) is C-U, (c) is C-PEG, (d) is C-EDTA, (e) is C-CA.

in the solution could affect the activity of the functional groups of additives. pH Variation in the impregnation solution was carried out in the presence of urea as chelating agents. The textural properties of nanocatalysts, the loading of Mo, and Ni on support were compared. The results of these experiments have been shown in Table 4.

The results proved that active metals loading in neutral pH are better than basic or acidic pH. Also, the most surface area is related to pH in the range of (5- 7). Specifically, the previous studies have shown that the morphology of MoO<sub>3</sub> in the presence of urea at pH = 7 is nanorod. In the basic pH, it is microrod, but it is nano spherical in the acidic pH. Therefore, it was concluded that nanorod morphology has the most surface area and loading on  $\gamma$ - Al<sub>2</sub>O<sub>3</sub> support. The results revealed that the increase in the pH from acidic to neutral improved the physical properties of the nanocatalysts. For more investigation, the XRD patterns of nanocatalysts obtained by urea in different pHs were compared. The XRD patterns of the nanocatalyst have been shown by decreasing the pH to the neutral and acidic solution. MoO<sub>3</sub> morphology leads to the nanoparticle with 3.4 nm and 3.7 nm, respectively.

Fig. 5 and Table 5 show the XRD patterns for the synthesized nanocatalysts in presence EDTA, urea in the various pHs, and no additive. The catalysts exhibit diffraction peaks at  $2\theta = 10^\circ$  to  $40^\circ$  attributed to the crystalline MoO<sub>3</sub> and NiO phases. No sharp peaks are detected at  $2\theta = 10^\circ$  to  $20^\circ$ , related to crystalline MoO<sub>3</sub> phase, in presence EDTA and acidic media, suggesting that the molybdenum oxide (MoO<sub>3</sub>) is highly dispersed over the  $\gamma$ - Al<sub>2</sub>O<sub>3</sub> support [35]. The prepared catalysts in presence urea and no additive show one diffraction peak in region of  $19^\circ$ . It can be concluded that dispersion of metals on support was being reduced. The diffraction peaks at  $2\theta = 31^\circ, 37^\circ, 39^\circ, 60^\circ$  are related to nanocrystals of MoO<sub>3</sub> that can be related to the MoO<sub>3</sub> with orthorombic phase [32]. Nanocrystals of nickel oxide (NiO) at  $2\theta = 37^\circ, 40^\circ, 45^\circ, 60^\circ$  and  $67^\circ$  are appeared [36,37]. Very broad diffraction peaks at  $46^\circ$  and  $66^\circ$  are due to the  $\gamma$ - Al<sub>2</sub>O<sub>3</sub> support. It is concluded that the impregnation of metals did not affect the  $\gamma$ -Al<sub>2</sub>O<sub>3</sub> crystalline phase of catalyst support [38]. Two peaks exist at  $2\theta = 45^\circ$  and  $67^\circ$  for NiO. They are close to specific peaks of  $\gamma$ -Al<sub>2</sub>O<sub>3</sub> and it can be interpreted as the overlap of defect NiO and  $\gamma$ -Al<sub>2</sub>O<sub>3</sub> [39].

**Table 4: Physicochemical properties of prepared catalysts with urea in the different media pH. The most surface area is related to pH in the range of (5- 7).**

| catalyst | BET                                            |                                                |                            | BJH                                            |                  |                                                | Chemical properties |       |
|----------|------------------------------------------------|------------------------------------------------|----------------------------|------------------------------------------------|------------------|------------------------------------------------|---------------------|-------|
|          | Surface Area (m <sup>2</sup> g <sup>-1</sup> ) | Pore Volume (cm <sup>3</sup> g <sup>-1</sup> ) | Average Pore Diameter (nm) | Pore Volume (cm <sup>3</sup> g <sup>-1</sup> ) | Pore Radius (nm) | Surface Area (m <sup>2</sup> g <sup>-1</sup> ) | MoO <sub>3</sub> %  | NiO % |
| C-U-3.5  | 218                                            | 0.6318                                         | 10.62                      | 0.6296                                         | 4.62             | 259.43                                         | 10.5                | 2.6   |
| C-U-5    | 254                                            | 0.72                                           | 11.30                      | 0.7064                                         | 3.54             | 253.5                                          | 29.66               | 3.62  |
| C-U-7    | 242                                            | 0.67                                           | 11.08                      | 0.6557                                         | 4.62             | 231.57                                         | 35                  | 4.42  |
| C-U-9    | 238.9                                          | 0.708                                          | 11.85                      | 0.6955                                         | 5.27             | 234                                            | 33.43               | 3.56  |

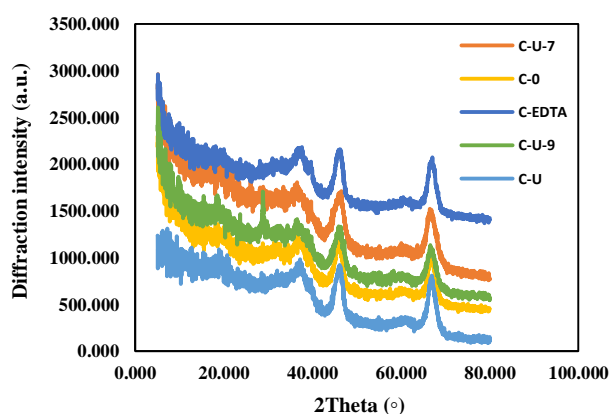


**Fig. 5: The XRD patterns for nano catalysts prepared in presence EDTA, urea in various pHs, and no additive. No sharp MoO<sub>3</sub> phase is detected, suggesting that the molybdenum oxide (MoO<sub>3</sub>) are highly dispersed over the  $\gamma$ -Al<sub>2</sub>O<sub>3</sub> support.**

After increasing pH to the basic media, the more characteristic diffraction peaks of MoO<sub>3</sub> are appeared, indicating the accumulation and enlarging in MoO<sub>3</sub> crystalline size. Also, a diffraction peak at 28.77° is appeared. This peak belongs to the NiMoO<sub>4</sub>, which might be formed during the catalyst preparation and it is not a good promoter for NiMoS-type structures [27]. To investigate the effect of pH on the size of MoO<sub>3</sub> crystals, the XRD pattern was used via debye-scherrer equation. Table 6 summarizes the results.

$$\tau = k\lambda / \beta \cos \theta \quad (6)$$

In the above equation,  $\tau$  is the size of Mo crystals,  $k$  is the crystal shape factor considered for spherical crystals. It is set equal to 0.94.  $\lambda$  is the x-ray wavelength corresponding to CuK $\alpha$  radiation (0.15406),  $\beta$  is the full width at half maximum (FWHM) of the Mo reflection. It is expressed in degrees, which should be converted

to the length unit, and  $\theta$  is the angle of diffraction corresponding to peak broadening.

As expected, the sharpest peak in XRD pattern belong to the nanocatalyst synthesized in basic media in comparison with neutral and acidic media possessing the largest crystal size (5 nm) because the morphology of MoO<sub>3</sub> in this catalyst is nanorod. By decreasing the pH to the neutral and acidic solution, MoO<sub>3</sub> morphology would lead to the nanoparticle with 3.4 nm and 3.7 nm, respectively [8]. These results were confirmed by the TPR patterns of the nanocatalysts synthesized in media with the comparison of acidic and basic pH.

#### TPR Results

The stability of the produced complex chelate agents with Ni is high in comparison with Mo. Furthermore, up to the temperature of 200°C, these chelating ligands started to decompose. Then Ni atoms sulfide were free up. They proceed the edges and corners of MoS<sub>2</sub> slabs and they create the active phases of Ni-Mo-S (type II). Moreover, since chelating agents reduce the interactions of metal and support, they increase the activity of the hydrotreating. More Ni-Mo-S active sites (type II) are formed [25]. Therefore, the reductive abilities of catalysts and strength interaction of metal-support in the different chelating agent and pH were studied by H<sub>2</sub>-TPR. The results are shown in Figs. 6 and 7. Hydrogen consumption is an index which exhibits catalyst performance, metal dispersion and active sites. Firstly, the effect of chelating agent on the metal-support interaction was investigated by TPR of nanocatalysts prepared in the absence and in the presence of EDTA, citric acid, urea as chelating agent. TPR profile of the NiMo/ $\gamma$ -Al<sub>2</sub>O<sub>3</sub> catalyst prepared without chelating agent has two reduction peaks in the low temperature range of (400-600)°C whose centers are at the temperatures

**Table 5: The information of the XRD patterns of synthesized nano catalysts in presence EDTA, urea in the various pHs, and no additive.**

| Catalyst | C-EDTA                 |              |                      | C-0           |                        |              |                      | C-U-5         |                        |              |                      | C-U-9         |                        |              |                      |               |
|----------|------------------------|--------------|----------------------|---------------|------------------------|--------------|----------------------|---------------|------------------------|--------------|----------------------|---------------|------------------------|--------------|----------------------|---------------|
|          | Pos. [ $^{\circ}$ Th.] | Height (cts) | d-spacing (observed) | Rel. Int. (%) | Pos. [ $^{\circ}$ Th.] | Height (cts) | d-spacing (observed) | Rel. Int. (%) | Pos. [ $^{\circ}$ Th.] | Height (cts) | d-spacing (observed) | Rel. Int. (%) | Pos. [ $^{\circ}$ Th.] | Height (cts) | d-spacing (observed) | Rel. Int. (%) |
|          | 31.9                   | 18           | 2.8                  | 5.36          | 19.2                   | 109          | 4.6                  | 32.71         | 19                     | 85           | 4.6                  | 25.04         | 18.71                  | 107          | 4.7                  | 34            |
|          | 37.09                  | 151          | 2.4                  | 44.5          | 31.9                   | 29           | 2.8                  | 8.8           | 32.5                   | 93           | 2.7                  | 27.15         | 28.77                  | 314          | 3.1                  | 100           |
|          | 39.52                  | 74           | 2.3                  | 21.77         | 37.31                  | 143          | 2.4                  | 42.9          | 36.9                   | 210          | 2.4                  | 61.59         | 36.97                  | 83           | 2.4                  | 26.44         |
|          | 45.93                  | 318          | 1.97                 | 93.72         | 45.85                  | 333          | 1.98                 | 100           | 39.6                   | 66           | 2.3                  | 19.48         | 39.1                   | 31           | 2.3                  | 9.79          |
|          | 60.5                   | 18           | 1.5                  | 5.23          | 59.98                  | 33           | 1.5                  | 9.86          | 45.9                   | 325          | 1.97                 | 95.43         | 46.03                  | 219          | 1.97                 | 69.73         |
|          | 66.84                  | 339          | 1.4                  | 100           | 66.77                  | 291          | 1.4                  | 87.47         | 60.7                   | 22           | 1.5                  | 6.47          | 49.39                  | 47           | 1.84                 | 14.96         |
|          |                        |              |                      |               |                        |              |                      |               | 66.8                   | 341          | 1.4                  | 100           | 58.14                  | 37           | 1.58                 | 11.81         |
|          |                        |              |                      |               |                        |              |                      |               |                        |              |                      |               | 60.1                   | 32           | 1.53                 | 10.10         |
|          |                        |              |                      |               |                        |              |                      |               |                        |              |                      |               | 66.71                  | 278          | 1.4                  | 88.69         |

**Table 6: The effect pH on morphology and crystal size of MoO<sub>3</sub> via debye- scherrer equation. By decreasing the pH to the neutral and acidic solution, MoO<sub>3</sub> morphology would lead to the smaller nanoparticle.**

| pH | 2 $\theta$ | $\theta$ | $\lambda$ | FWHM | cos $\theta$ | $\beta$ | $d_{p, XRD}$ | Crystal size of MoO <sub>3</sub> (nm) | Peak height of MoO <sub>3</sub> in XRD |
|----|------------|----------|-----------|------|--------------|---------|--------------|---------------------------------------|----------------------------------------|
| 5  | 37.26      | 18.63    | 0.15406   | 2.3  | 0.976        | 0.040   | 3.7          | 3.7                                   | 154                                    |
| 7  | 36.9       | 18.45    | 0.15406   | 2.6  | 0.921        | 0.045   | 3.4          | 3.4                                   | 117                                    |
| 9  | 36.9       | 18.45    | 0.15406   | 1.8  | 0.921        | 0.031   | 5            | 5                                     | 153                                    |

of 455°C and 560°C. This is due to weak and strong interactions of Mo/ $\gamma$ -Al<sub>2</sub>O<sub>3</sub> support, respectively. Furthermore, a high temperature reduction peak is located at 840°C because of the Ni-support. When EDTA was added during preparation of catalyst, TPR profile is changed and reduction peak of Mo species is moved to a lower region of the temperature. The reduction temperatures were 33°C and 10°C for octahedral and tetrahedral Mo<sup>6+</sup>, respectively. It means EDTA causes weak interaction between metal / $\gamma$ -Al<sub>2</sub>O<sub>3</sub> support leading to high activity of catalyst and strong interaction in the Ni / $\gamma$ -Al<sub>2</sub>O<sub>3</sub> support. The reduction peak is shifted to a higher temperature that suggests Ni with more stable bond on  $\gamma$ -Al<sub>2</sub>O<sub>3</sub> support. Two peaks are due to both tetrahedral and octahedral Mo<sup>6+</sup> species. The tetrahedral Mo<sup>6+</sup>/  $\gamma$ -Al<sub>2</sub>O<sub>3</sub> interaction is stronger than the one between octahedral Mo<sup>6+</sup> and  $\gamma$ -Al<sub>2</sub>O<sub>3</sub>. Hence, the first peak located at the low

temperature region is due to the partial reduction of octahedral Mo<sup>6+</sup> species to Mo<sup>4+</sup> and small crystalline structure of MoO<sub>3</sub>. The high temperature region has a peak (the second one) showing the reduction that belongs to tetrahedral Mo<sup>6+</sup> species and the further reduction of MoO<sub>2</sub> from Mo<sup>4+</sup> to Mo<sup>0</sup>. The TPR results of the synthesized catalysts in the different pH prove that the application of citric acid and urea as a chelating agent and hydrogen consumption in acidic pH is more compared to basic pH. Furthermore, in the acidic pH, the reductive abilities of catalysts are similar when urea and citric acid are used. In the basic pH, citric acid is better compared to urea as chelating agent. Correspondingly, it can be concluded that in the acidic pH with both of chelating agents, H<sub>2</sub>- consumption is more compared to basic pH. In the acidic pH, metal dispersion on support, active sites, and the reductive abilities of catalysts were better compared

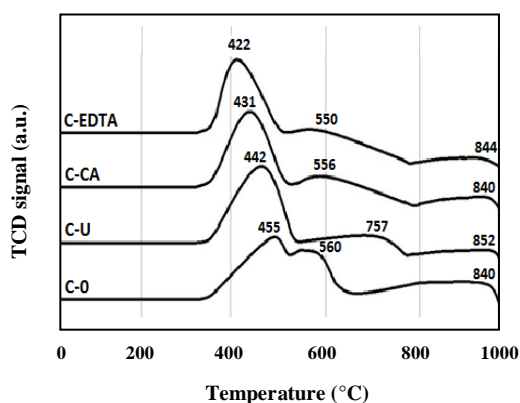


Fig. 6: TPR profiles of samples prepared by different chelate agents. EDTA adding causes weak interaction between metal / $\gamma$ - $\text{Al}_2\text{O}_3$  support, and strong interaction in the Ni / $\gamma$ - $\text{Al}_2\text{O}_3$  support.

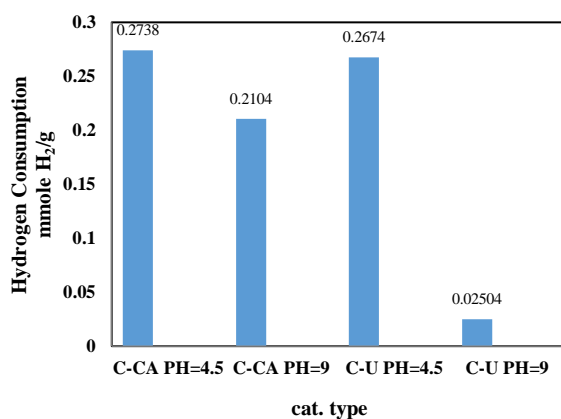


Fig. 7: TPR profiles of samples prepared by using urea and citric acid in the acidic and basic pH. Hydrogen consumption in acidic pH is more compared to basic pH.

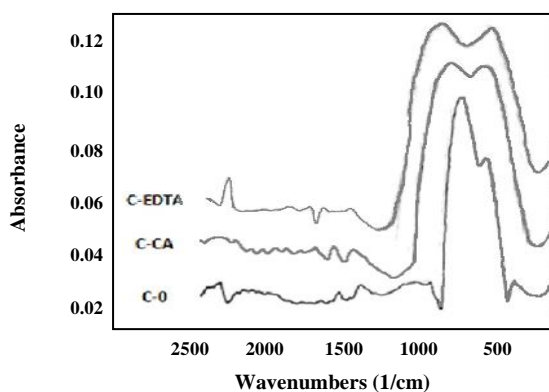


Fig. 8: FTIR spectra of the C-0, C-CA, C-EDTA catalysts and comparing of height of the absorbance peaks of them.

to a medium with basic pH. The comparative TPR analysis for nanocatalysts using urea and citric acid in the acidic and basic pH is shown in Fig. 7 [20].

### FT-IR Results

FT-IR spectrum of NiMo/ $\gamma$ - $\text{Al}_2\text{O}_3$  catalyst indicates two peaks due to the absorbance of Ni-site ( $590\text{-}630\text{ cm}^{-1}$ ), Mo-site ( $790\text{-}820\text{ cm}^{-1}$ ). The absorption of region  $817.63\text{ cm}^{-1}$  in the C-0 catalyst and region of  $784.53\text{ cm}^{-1}$  in the C-CA, C-EDTA catalysts exist because Mo-site do not change much. The absorption of region  $593.92\text{ cm}^{-1}$  in the C-CA, C-EDTA catalysts can be related to Ni-site compared with peaks of  $632.54\text{ cm}^{-1}$  accompanied by a significant increase. Therefore, the analysis was about chelate agent effective on Ni and the formation of a stable complex with Ni in comparison with Mo and releasing in the above temperature was confirmed. So, we can conclude the mentioned increase is apparently higher if the catalyst was prepared by using chelating agents with the following order: EDTA > CA > none. This order is completely confirmed with the HDS activity order. One can suggest that metals are highly dispersed and much metal sites can be generated over the surface if the catalysts are prepared with the chelating agents. It was found that the number of active sites is higher in more active catalysts [27]. Fig. 8 shows FT-IR peaks around region of the metals.

### Activity and stability tests

Firstly, to compare the activity of catalysts, a real HDS was conducted with catalysts synthesized in acidic pH with EDTA, citric acid, urea, and no-additive. Then, they were compared with a commercial catalyst. The mixed system of heavy oil and gas oil was applied as a feedstock of hydrotreating. The catalytic activity was measured as a function of removal percentage of the present sulfur compounds in the feed. After desulfurization process, amount of total sulfur in the feed is determined by Rikagu devices. Table 7 shows the result of reducing of sulfur in the feed. The HDS reaction was conducted in a continuous fixed bed reactor operating at laboratory pressure of 60 bar,  $1.5\text{ h}^{-1}$  LHSV, and  $\text{H}_2/\text{H.C.}$  ratio of 1000 ppm at  $380^\circ\text{C}$  with 5g catalyst [25]. The HDS conversions for the catalysts and comparison with commercial catalyst are presented in Fig. 9.

Table 7: The sulfur in the feed after desulfurization.

| catalyst | S (grL <sup>-1</sup> ) after HDS | Sulfur conversion |
|----------|----------------------------------|-------------------|
| C-0      | 4.17                             | 80.14             |
| C-U      | 3.3                              | 84.28             |
| C-CA     | 2.4                              | 88.57             |
| C-EDTA   | 2                                | 90.47             |
| C-comm.  | 1.2                              | 94.28             |

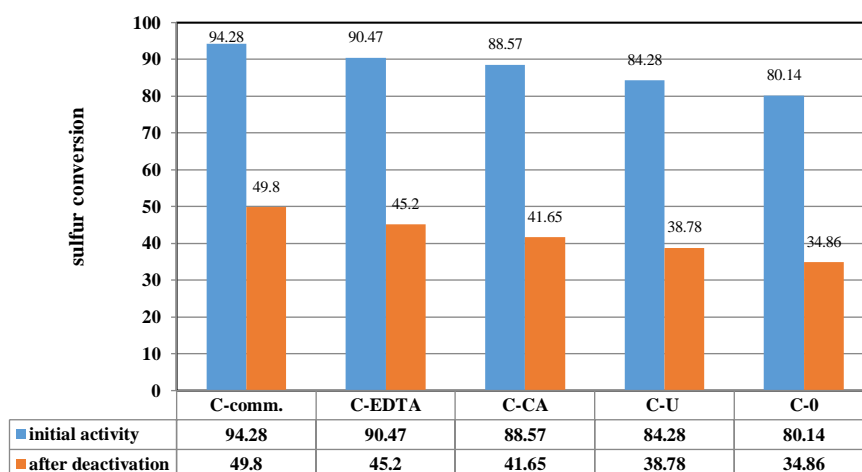


Fig 9: Comparing the results of HDS activity and accelerated deactivation of synthesized catalysts with/without chelate agent and commercial catalyst.

The stability of the catalyst depends upon interaction of support – active metal. If the precursor concentration is low, these interactions will cause the surface absorption of metal anion on support. Additionally, more concentration of precursor, aggressive species on support becomes crystalline after drying. There are two types of phases for Ni-Mo-S [40]. The type I phase was built up from Ni-Mo-S, with strong interaction between support and active metal and less sulfonation (causes bonding of Mo-Al-O). In the phase II of Ni-Mo-S, all particles are sulfurized and kept on  $\gamma$ -Al<sub>2</sub>O<sub>3</sub> support by van der waals forces. Phase II is more active and less stable than phase I. In this catalyst, the application of chelate agent results in forming of Ni-Mo-S active phase II on  $\gamma$ -Al<sub>2</sub>O<sub>3</sub> support and active species is distributed on  $\gamma$ -Al<sub>2</sub>O<sub>3</sub> surface. Chelate additives help to distribute active species on  $\gamma$ -Al<sub>2</sub>O<sub>3</sub> support and to decrease the interaction between Mo, Ni with  $\gamma$ -Al<sub>2</sub>O<sub>3</sub> support until the formation of the sulfide active phase II [41,42,25]. In addition, in presence of the chelate ligand,

at the higher temperature, sulfonation of Ni began after the sulfonation of Mo or simultaneously. Accordingly, it is possible that Ni is taken in edges of MoS and increased active phase Ni-Mo-S. Therefore, the possibility of CO separation decreases individually [43].

The activity of catalysts during the reactions is changed and reduced with time in the petroleum refineries. Rate of deactivation is important and different for various catalysts. For evaluation of catalyst performance or stability, it should be performed similarly to the refinery process in the pilot plant. For this reason, accelerated deactivation technique is used [44].

In the hydrotreating catalysts, deactivation occurs mainly due to the poisoning and closure of the catalyst pores with toxic metals such as vanadium and nickel in the heavy oil and sintering of active sites and coke formation on the catalyst surfaces. The references indicate that catalyst activity in the hydrotreatment process of gas oil in a working cycle is reduced by 20% [45,46]. The results

of accelerated deactivation of synthesized catalysts with and without the presence of the chelate agent and commercial catalyst have shown that conversion of catalyst in HDS process was decreased after deactivation of catalyst, but the rate of catalytic activity reduction is almost identical for all the catalysts, and is similar to the commercial catalyst. It was concluded that additives do not affect deactivation.

## CONCLUSIONS

In this research, various NiMo/ $\gamma$ -Al<sub>2</sub>O<sub>3</sub> nanocatalysts in presence of various chelating agents were prepared and were used as HDS catalyst. The physicochemical properties of catalysts were characterized by TPR, BET, BJH, AAS, FT-IR, XRD and SEM techniques. The properties of catalysts with chelate agent in comparison with non- chelate agent catalysts were improved. In that case, the synthesized catalyst in presence EDTA with six dents has represented the maximum sulfur conversion (90.47%), minimum interaction between active metal and support, and the most surface area (250 m<sup>2</sup>/g), and the smallest particle size. Also, variety of pH media showed neutral pH toward basic and acidic pH, the increase in loading of Mo, Ni nanoparticle on the  $\gamma$ -Al<sub>2</sub>O<sub>3</sub> support. However, pH=5 reveals the highest surface area of 254 m<sup>2</sup>/g. By decreasing the pH to the neutral and acidic solution, MoO<sub>3</sub> morphology leads to the nanoparticle with the sizes of 3.4 nm and 3.7 nm, respectively. Then, in the acidic pH, metal dispersion on support, active sites and the reductive abilities of catalysts were better compared to a medium with basic pH. Ultimately, it can be concluded that among the supported NiMo hydrotreating catalysts, synthesized nanocatalysts in presence of chelating agents revealed comparable HDS activities. Consequently, C-EDTA had the specified physicochemical properties to be an appropriate hydrotreating catalyst.

## Acknowledgments

The authors would like to thank of the Mrs. Zahra Shahidian and Mrs. Sara Beshkoofeh from the Iranian Institute of Research and Design in Chemical Industries (IRDCI) for his support.

Received : Jul. 9, 2019 ; Accepted : Oct. 28, 2019

## REFERENCES

- [1] Huang Z.D., Bensch W., Lotnyk A., Kienle L., Fuentes S., Bocarando J., Alonso G., Ornelas C., [SBA-15 as Support for NiMo HDS Catalysts Derived from Sulfur-Containing Molybdenum and Nickel Complexes: Effect of Activation Mode](#), *J. mole. Catal. A: Chemical* **323**: 45-51(2010)
- [2] Bej S.K., Maity S.K., Turaga U.T., [Search for an Efficient 4-6-DMDBT Hydrodesulfurization Catalyst](#), *Ener. & Fuels* **18**:1227-1237 (2004)
- [3] Escobar J., De Los Reyes J.A., Ulin C. A., Barrera M.C., [Highly Active Sulfide CoMo Catalysts Supported on \(ZrO<sub>2</sub>- TiO<sub>2</sub>\)/Al<sub>2</sub>O<sub>3</sub>](#), *Mate. Chem. and Phys.* **143**: 213-222 (2013)
- [4] Pawelec B., Navarro R.M., Campos – Martin J.M., Lopez Agudo A. Vasudevan P.T., Fierro J.L.G., [Silica- Alumina – Supported Transition Metal Sulfide Catalysts for Deep Hydrodesulfurization](#), *Catal. Today* **86**: 73-85 (2003)
- [5] Shahidian Z., Zare K., Moosavi M., [Modification of Mesoporous Extrudate Gamma Alumina through Thermal Ammonia Treatment](#), *Iran. J. Chem. Chem. Eng. (IJCCE)*, **39**(3): 61-69 (2019).
- [6] Badoga S., Sharma R.V., Dalai A.K., Adjaye J., [Synthesis and Characterization of Mesoporous Aluminas with Different Pore Sizes: Application in Nimo Supported Catalyst for Hydrotreating of Heavy Gas Oil](#), *Appl. Catal. A: General* **489**: 86-97 (2015)
- [7] Shahidian Z., Zare K., Moosavi M., [Improvement of Heavy Oil Hydrodesulfurization Catalyst Support Properties by Acetic Acid Treatment](#), *Iran. J. Chem. Chem. Eng. (IJCCE)*, **39**(3): 71-80 (2019)
- [8] Parviz D., Kazemeini M., Rashidi A.M., Jafari Jozani Kh., [Synthesis and Characterization of MoO<sub>3</sub> Nanostructures by Solution Combustion Method Employing Morphology and Size Control](#), *J. Nanopart. Res.* **12**:1509-1521 (2010)
- [9] Liu H., Liu C., Yin C., Chai Y., Li Y., Liu D., Liu B., Li X., Wang Y., Li X., [Preparation of Highly Active Unsupported Nickel – Zinc- Molybdenum Catalysts for the Hydro Desulfurization of Dibenzothiophene](#), *Appl. Catal. B: Environmental* **174-175**: 264-276 (2015)
- [10] Yi Y., Zhang B., Jin X., Wang L., Williams C.T., Xiong G., Su D., Liang C. [Unsupported NiMoW Sulfide Catalysts for Hydro Desulfurization of Dibenzothiophene by Thermal Decomposition of Thiosalts](#), *J. Mol. Catal. A: Chemical*, **351**:120-127 (2011).

- [11] Eijsbouts S., Mayo S.W., Fujita K., **Unsupported Transition Metal Sulfide Catalysts: from Fundamentals to Industrial Application**, *Appl. Catal. A: General* **322**: 58-66 (2007).
- [12] Mandal S., Lahiri S., **Synthesis of Molybdenum Nanoparticle by *in Situ*  $\gamma$ -Radiation**, *Appl. Rad. and Iso.* **70**: 2340 – 2343(2012)
- [13] Kisszekelyi P., Alammari A., Kupai J., Husztly P., Barabas J., Holtzl T., Szente L., Bawn C., Adams R., Szekely G., **Asymmetric Synthesis with Cinchona-Decorated Cyclodextrin in a Continuous-Flow Membrane Reactor**, *J. Catal.*, **371**: 255-261(2019).
- [14] Didaskalou C., Kupai J., Cseri L., Barabas J., Vass E., Holtzl T., Szekely G., **Membrane – Grafted Asymmetric Organocatalyst for an Integrated Synthesis-Separation Platform**, *ACS Catal.* **8**: 7430-7438 (2018).
- [15] Valencia D., Klimova T., **Kinetic Study of NiMo/SBA-15 Catalysts Prepared with Citric Acid in Hydrodesulfurization of Dibenzothiophene**, *Catal. Commun.* **21**: 77-81 (2012).
- [16] Sun M., Nicosia D., Prins R., **The Effects of Fluorine, Phosphate and Chelating Agents on Hydrotreating Catalysts and Catalysis**, *Catal. Today* **86**:173-189 (2003).
- [17] Shimizu T., Hiroshima K., Honma T., Mochizuki T., Yamada M., **Highly Active Hydrotreatment Catalysts Prepared with Chelating Agents**, *Catal. Today* **45**: 271-276 (1998).
- [18] Kishan G., Coulier L., de Beer V.H.J., Van Veen J.A.R., Niemantsverdriet J.W., **Sulfidation and Thiophene Hydrodesulfurization Activity of Nickel Tungsten Sulfide Model Catalysts, Prepared Without and with Chelating Agents**, *J. Catal.* **196**: 180-189 (2000).
- [19] Suarez-Toriello V.A., Santolalla-Vargas C.E., de los Reyes J.A., Vazquez-Zavala A., Vrinat M., Geantet C., **Influence of the Solution Ph in Impregnation with Citric Acid and Activity of Ni/W/Al<sub>2</sub>O<sub>3</sub> Catalysts**, *J. Mol. Catal. A Chem.* **404**: 36-46 (2015).
- [20] Singh R., Kunzru D., Sivakumar S., **Monodispersed Ultrasmall NiMo Metal Oxide Nanoclusters as Hydrodesulfurization Catalyst**, *Appl. Catal. B: Environmental*, **185**: 163–173 (2016).
- [21] Hocevar B., Grilc M., Hus M., Likozar B., **Mechanism, *Ab initio* Calculations and Microkinetics of Straint-Chain Alcohol, Ether, Ester, Aldehyde, and Carboxylic Acid Hydrodeoxygenation over Ni-Mo/Al<sub>2</sub>O<sub>3</sub> Catalyst**, *Chem. Eng. J.*, **359**: 1339-1351(2018).
- [22] Hocevar B., Grilc M., Hus M., Likozar B., **Mechanism, *ab Initio* Calculations and Microkinetics of Hydrogenation, Hydrodeoxygenation Double Bond Migration and Cis-Trans Isomerisation During hydrotreatment of C<sub>6</sub> secondary Alcohol Species and Ketones**, *Appl. Catal. B: Environmental*, **218**: 147-162 (2017).
- [23] Grilc M., Likozar B., **Levulinic Acid Hydrodeoxygenation, Decarboxylation and Oligomerization over Ni-Mo/ Al<sub>2</sub>O<sub>3</sub> Catalyst to Bio-Based Value-Added Chemicals: Modeling of Mass Transfer, Thermodynamic and Micro-Kinetics**, *Chem. Eng. J.*, **330**: 383-397(2017).
- [24] Khadem-Hamedani B., Yaghmaei S., Fattahi M., Mashayekhan S., Hoseini-Ardali S.M., **Mathematical Modeling of a Slurry Bubble Column Reactor for Hydrodesulfurization of Diesel Fuel: Single- and Two-Bubble Configuration**, *Chem. Eng. Res. Des.*, **100**: 362-376 (2015).
- [25] Dr. Ajay Dalai, Dr. John Adjaye, Head of the Department, Chemical and Biological Engineering, University of Saskatchewan, 57 Compus Drive, Saskatoon, Saskatchewan, Canada S7N5A9.
- [26] Hiroshima K., Mochizuki T., Honma T., Shimizu T., Yamada M., **High HDS Activity of Co-Mo / Al<sub>2</sub>O<sub>3</sub> Modified by Some Chelates and Their Surface Fine Structures**, *Appl. Surf. Sci.* **121/122**: 433-436 (1997).
- [27] Mazoyer P., Geantet C., Diehl F., Loridant S., Lacroix M., **Role of Chelating Agent on the Oxidic State of Hydrotreating Catalysts**, *Catal. Today* **130**: 75-79 (2008).
- [28] Daag M., Chianlli R.R., **Structure-Function Relations in Molybdenum Sulfide Catalysts: the ‘Rim-Edge’ Model**, *J. of Catal.*, **149**: 414-427 (1994).
- [29] Jeziorowski H., Knozinger H., **Raman and Ultraviolet Spectroscopic Characterization of Molybdenum on Alumina Catalysts**, *J. Phys. Chem.*, **83**: 1166 (1979).
- [30] Payen E., Grimblot j., Kasztelan S., **Study of Oxidic And Reduced Alumina- Supported Molybdate and Heptamolybdate Species by *in Situ* Laser Raman Spectroscopy**, *J. Phys. Chem.*, **91**: 6642 – 6648 (1987).
- [31] Hu H., Wachs I.E., Bare S.R., **Surface Structures of Supported Molybdenum Oxide Catalysts: Characterization by Raman and Mo L<sub>3</sub>- Edge XANES**, *J. Phys. Chem.* **99**:10897-10910 (1995).

- [32] Escobar J., Barrer M., Gutierrez A., Cortes-Jacome M., Angeles-Chavez A., Toledo J., Solis-Casados D., Highly Active P-doped Sulfided NiMo/Alumina HDS Catalysts from Mo-blue by Using Saccharose as Reducing Agents Precursor, *Appl. Catal. B: Environmental*, **237**: 708–720 (2018).
- [33] Ohman L. O., Equilibrium and Structural Studies of Silicon (IV) and Aluminum (III) in Aqueous Solution. A Potentiometric and  $^{27}\text{Al}$  NMR Study of System  $\text{H}^+$ -  $\text{Al}^{3+}$ -  $\text{MoO}_4^{2-}$ , *Inorg. Chem.* **28**: 3629-3632 (1989)
- [34] Bihan L.L., Blanchard P., Fournier M., Grimblot J., Payen E., Raman Spectroscopic Evidence for the Existence of 6-Molybdoaluminate Entities on an  $\text{Mo}/\text{Al}_2\text{O}_3$  Oxidic Precursor, *J. Chem. Soc. Faraday Trans.*, **94**: 937-940 (1998).
- [35] Al-Megren H., Huang Y., Chen H., Alkinany M., Gonzalez-Cortes S., Aldrees S., Xiao T., Effect of Urea/Metal Ratio on the Performance of NiMoP/ $\text{Al}_2\text{O}_3$  Catalyst for Diesel Deep HDS, *Appl. Petrochem Res.*, **5**: 173-180 (2015).
- [36] Valencia D., Klimova T., Effect of the Support Composition on the Characteristics of NiMo and CoMo/(Zr) SBA-15 Catalysts and their Performance in Deep Hydrodesulfurization, *Catal. Today* **166**: 91-101 (2011).
- [37] Zhang D., Duan A., Zhao Z., Gao G., Jiang G., Chi K., Chuang K.H., Preparation, Characterization and Hydrotreating Performance of  $\text{ZrO}_2$ -  $\text{Al}_2\text{O}_3$  Supported NiMo Catalysts, *Catal. Today*, **149**: 62-68 (2010).
- [38] Choi J., Yoo K.S., Kim S.D., Park H.K., Chul-Woo Nam C.W., Jinsoo Kim J., Synthesis of Mesoporous Spherical  $\gamma$ - $\text{Al}_2\text{O}_3$  Particles with Varying Porosity by Spray Pyrolysis of Commercial Boehmite, *J. Ind. Eng. Chem.*, **56**: 151-156 (2017).
- [39] Valencia D., Klimova T., Citric Acid Loading for  $\text{MoS}_2$  – Based Catalysts Supported on SBA-15 New Catalytic Materials with High Hydrogenolysis Ability in Hydrodesulfurization, *Appl. Catal. B* **129**: 137-145 (2013).
- [40] Van Veen J.A.R., Colijn H.A., Hendriks P.A.J.M., Vanwelsen A.J., On the Formation of Type I and Type II NiMoS Phases in NiMo/ $\text{Al}_2\text{O}_3$  Hydrotreatment catalysts and Its Catalytic Implications, *Fuel proc. Tech.*, **35**: 137-157 (1993).
- [41] Blanchard P., Lamonier C., Griboral A., Payen E., New Insight in the Preparation of Alumina Supported Hydrotreatment Oxidic Precursors: A Molecular Approach, *Appl. Catal. A: General*, **322**: 33 – 45 (2007).
- [42] Al-Dalama K., Stanislaus A., A Comparative Study of Influence of Chelating Agents on the Hydrodesulfurization (HDS) Activity of Alumina and Silica-Alumina-Supported CoMo Catalysts, *Energy & Fuels*, **20**: 1777-1783 (2006).
- [43] Pashigreva A.V., Bukhtiyarova G.A., Klimov O.V., Chesalov Y.A., Litvak G.S., Noskov A.S., Activity and Sulfidation Behavior of the CoMo / $\text{Al}_2\text{O}_3$  Hydrotreating Catalyst: the Effect of Drying Condition, *Catal. today*, **149**: 19-27 (2010).
- [44] Venkatesh P., Bhaskar M., Sakthivel S., Selvaraju N., Pilot Plant Studies on Accelerated Deactivation of Commercial Hydrotreating Catalyst, *Petro. Scie. Tech.*, **28**: 93-102 (2010).
- [45] Fatemi S., Abolhamd G., Moosavian M.A., Mortazavi Y., The Effect of Coking on Kinetics oh HDS Reaction under Steady and Transient States, *Iran. J. Chem. Chem. Eng.(IJCCCE)*, **23(2)**: 1-11 (2004).
- [46] Remesat D., Young B., Svrcek W.Y., Improving Vacuum Gas Oil Hydrotreating Operation via a Lumped Parameter Dynamic Simulation Modeling Approach, *Chem. Eng. Res. Des.*, **87**: 153-165 (2009).